Chemistry–A European Journal
Research Article
doi.org/10.1002/chem.202201425
Chemistry Europe
European Chemical Societies Publishing
www.chemeurj.org

Chemiluminescent Imaging Assay of SARS-CoV-2 Protein with Target-Induced Enzyme Activity Regulation

Special Collection

Yuhui Chen,[a] Hang Ao,[a] Wencheng Xiao,[a] Huangxian Ju,*[a] and Jie Wu*[a]

Dedicated to the 120th anniversary of Nanjing University

Abstract: Simple but robust testing assays are essential for screening and diagnosis of individuals infected with severe acute respiratory syndrome coronavirus 2 (SARS-CoV-2) in COVID-19 pandemic. Here, we described a chemiluminescent imaging assay (CLIA) for sensitive and convenient detection of SARS-CoV-2 nucleocapsid protein (NP) by a target-induced enzyme activity regulation (T-EAR) strategy. The T-EAR used a pair of antibody-DNA probes to recognize SARS-CoV-2 NP and proximity-induce rolling circle amplification for mass-production of pyrophosphate to coordinate with Cu^{2+}, which prevented the reduction of Cu^{2+} to Cu^{+} by sodium ascorbate as well as the Cu^{+}-caused inactivation of horseradish peroxidase (HRP). The activity retention of HRP produced strong CL signal for the detection of SARS-CoV-2 NP by catalyzing the oxidation of luminol by H_2O_2. The T-EAR based CLIA showed a wide detection range from 1 pg/mL to 100 ng/mL (13 fM to 1.3 nM) with the requirement of only 0.75 μL of sample. This CLIA had advantages of good sensitivity, simple wash-free operation, acceptable accuracy, and high-throughput imaging detection, displaying potential applicability in screening assay of COVID-19 infection.

Introduction

The continued spread of coronavirus disease 2019 (COVID-19) caused by severe acute respiratory syndrome coronavirus 2 (SARS-CoV-2) has resulted in several million deaths and tremendous economic losses. Due to the high human-to-human transmissibility of SARS-CoV-2, sensitive and convenient detection methods are urgently needed for population-wide screening to identify the infected individuals, which is essential for containing the spread of COVID-19. The current gold standard test of SARS-CoV-2 infection is real-time polymerase chain reaction (RT-PCR) assay of SARS-CoV-2 virus-specific sequences, however, this diagnosis assay requires a long turnaround time with skilled technicians. In addition, some research have also reported that RT-PCR test is not suitable for all patients and cannot provide adequate information on progression of the disease.[1]

Recently, detection of SARS-CoV-2 antigens including nucleocapsid protein (NP) and spike protein (SP) in sera and nasopharyngeal secretions is considered as a good alternative to RT-PCR of viral RNA for accurate diagnosis.[2] It's worth noting that NP is extensively used in leading serodiagnostics kits due to its abundant expression during infection and early antibody response. Commercial antigen testing kits are developed mainly based on lateral flow immunoassay (LFIA) and magnetic bead immunoassay (MBIA), however, most of them still have defects in practical diagnosis. For example, although LFIA-based testing kits can achieve convenient, low-cost and rapid detection of SARS-CoV-2 antigens, it often lacks sensitivity for early and prompt screening of COVID-19.[3] In contrast, MBIA-based testing kits can provide good detection sensitivity, but they suffer from multiple wash and separation steps, thus automated instrument and laboratory operation are required, which is not suitable for large-scale infection screening.[4] Hence, the development of assays with simple operation, rapid detection and high sensitivity is still of great significance for testing of SARS-CoV-2 antigens.

Proximity binding-based immunoassay (PBIA) is a newly developed protein detection with DNA technology.[5] In PBIA, the target protein is sandwich recognized by a pair of DNA-based affinity probes to form proximity ligation product and generate amplifiable DNA strands for detection. Normally, PBIA combines with mature DNA amplification strategies, such as PCR, rolling circle amplification (RCA), catalytic hairpin assembly (CHA) and hybridization chain reaction (HCR), to design superior assays for simple, specific and sensitive detection of proteins.[6] Particularly, homogeneous fluorescent PBIA has been reported to achieve the sample-in-answer-out detection of immune proteins.[7] However, fluorescent assay has the drawback in analysis of serum samples due to the interference of autofluorescence from biological molecules.

Chemiluminescent (CL) assay, in which luminescence signal is produced by specific chemical reactions, is ideal for serologic detections due to the advantages of low background, high

[a] Y. Chen, H. Ao, W. Xiao, Prof. H. Ju, Prof. J. Wu
State Key Laboratory of Analytical Chemistry for Life Science
School of Chemistry and Chemical Engineering
Nanjing University, Nanjing 210023 (China)
E-mail: hxju@nju.edu.cn
wujie@nju.edu.cn

Supporting information for this article is available on the WWW under https://doi.org/10.1002/chem.202201425

Special Collection This manuscript is part of a Special Collection dedicated to the 120th Anniversary of Nanjing University.

sensitivity, low cost, easy operation and simple instruments.[8] For example, CL PBIAs have been established for wash-free detection of protein biomarkers at low concentration in complex samples.[9] On the other hand, CL imaging assay (CLIA) has the unique ability of high throughput and operation convenience in multiplexed assays.[10] Lately, a CLIA has been designed for wash-free and sensitive detection of SARS-CoV-2 NP with the combination of PBIA and RCA-assisted G-quadruplex/hemin DNAzyme formation. Although the results have shown it could detect fg/mL-level SARS-CoV-2 antigen, the robustness of DNAzyme-based CLIA is challenged because of the fast luminescence and instability of DNAzyme.[11]

Horseradish peroxidase (HRP)-luminol-H_2O_2 system is the most developed and robust CL system, and has been widely used in CLIA.[12] However, due to the lack of effective enzymatic switch, most HRP-based CLIAs are heterogeneous systems and include multiple washing operations.[13] In this work, we designed a target-induced enzyme activity regulation (T-EAR) strategy to develop a homogeneous HRP-based CLIA for convenient and sensitive detection of SARS-CoV-2 NP. In T-EAR, SARS-CoV-2 NP was double recognized by a pair of antibody-DNA probes to proximity-induce RCA process in which large amount of pyrophosphate anions (PPi) was produced to down-regulate the reduction of Cu^{2+} to Cu^{+}, and finally up-regulate the retention of active HRP. The activity retention of HRP produced strong CL signal for target detection. The proposed CLIA could be carried out with only 0.75 μL of sample and showed a wide detection range from 1 pg/mL to 100 ng/mL (13 fM to 1.3 nM) for SARS-CoV-2 NP. The T-EAR based CLIA was sensitive and simple, and could be high-throughput imaging detection, showing promise applicability in COVID-19 infection screening.

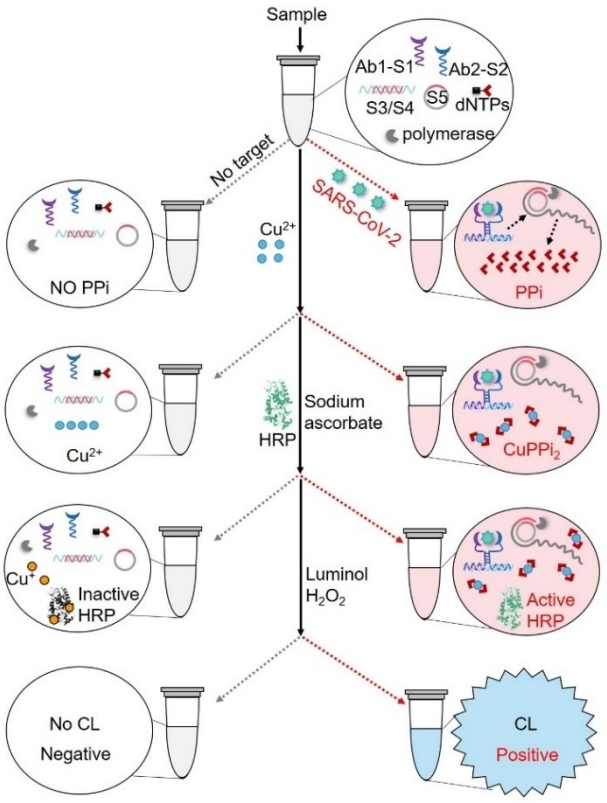

Scheme 1. Schematic Illustration of the CLIA of SARS-CoV-2 NP via target-Induced enzyme activity regulation strategy.

Results and Discussion

The CLIA of sample only needed four solution addition steps without any wash and separation operations (Scheme 1). Step 1, add sample into the assay solution, which contained a pair of affinity probes (Ab1-S1 and Ab2-S2), a primer blocked dsDNA (S3/S4) (Table S1), a circular DNA (S5), phi 29 polymerase, and dNTPs. Here, if the sample was SARS-CoV-2 NP positive, a sandwich immune-complex with a proximity-ligated oligonucleotide sequence (Ab1-S1/SARS-CoV-2 NP/Ab2-S2) was firstly formed by the target-induced proximity hybridization of S1 and S2. This proximity-ligated sequence could hybridize with block DNA (S4) to release primer DNA (S3) from S3/S4 dsDNA. The free S3 then hybridized with S5 to initiate an RCA process in which a huge mass of PPi was produced. Step 2, addition of Cu^{2+}. As PPi was an excellent chelate agent for metal ions, $Cu(P_2O_7)_2^{6-}$ complex ($CuPPi_2$) would be formed in the positive test tube.[14] Step 3, addition of the mixture of native HRP and sodium ascorbate (SA). In the SARS-CoV-2 NP negative tube, SA reduced free Cu^{2+} to Cu^{+} which then inactivated HRP through the interaction of Cu^{+} with amino acid residues in HRP.[15] In contrast, in the SARS-CoV-2 NP positive tube, the formation of $CuPPi_2$ hindered the reduction of Cu^{2+} to Cu^{+}, which restored the enzymatic activity of HRP. Step 4, addition of CL substrate, a mixture of luminol and H_2O_2, for CL signal generation by active HRP. In this T-EAR, the retention rate of active HRP was positively correlated with the levels of target protein, hence it was used to construct CLIA of SARS-CoV-2 NP.

In this work, the T-EAR was designed based on a PPi-mediated HRP activity regulation (Figure 1A). Cu^{+} was a well-known HRP inhibitor and could inhibit HRP activity effectively.[15] Additionally, Cu^{+} could be in situ produced by the reduction of Cu^{2+} with SA. Thus, active HRP would transform to inactive HRP when it coexisted with Cu^{2+} and SA, leading to the decrease of CL intensity in the mixture of luminol and H_2O_2 (Figure 1B, column d). Although SA alone was reported to have bare effect on the catalytic ability of HRP,[14b] it affected the CL intensity of HRP-luminol-H_2O_2 system (Figure 1C). This might be because the SA would move the solution to a low pH with the increase of its concentration, which was unfavorable to HRP-luminol-H_2O_2 CL system. In this work, 5 μM SA was used because SA at this concentration showed a slight effect on CL intensity (Figure 1B, column b). On the other hand, no obvious CL change was observed when active HRP was mixed only with Cu^{2+} (Figure 1B, column c), indicating the inhibition ability of Cu^{2+} was much lower than Cu^{+} and could be ignored in this work.[14c] Interestingly, the transformation of active HRP to inactive HRP in the coexistence of Cu^{2+} and SA could be hindered by PPi, who would protect Cu^{2+} from the

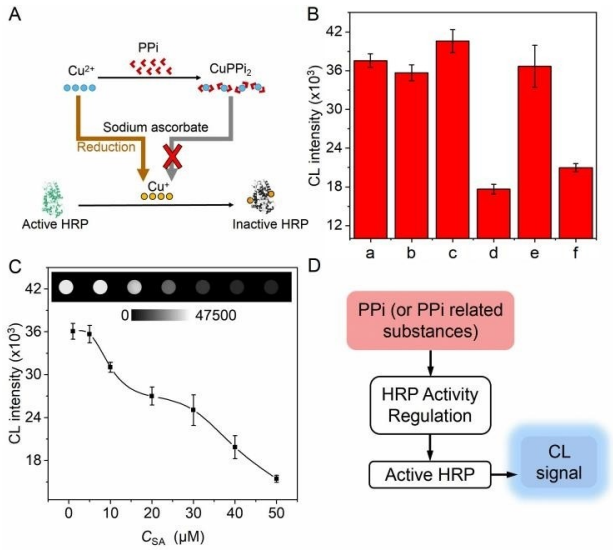

Figure 1. A) Schematic diagram of the PPi-mediated HRP activity regulation. B) CL intensities of the mixtures prepared by separate addition of 20 μL enzyme solutions of HRP (a), HRP + SA (b), HRP + Cu^{2+} (c), HRP + SA + Cu^{2+} (d), PPi + Cu^{2+} + SA + HRP (e), and dNTP + Cu^{2+} + SA + HRP (f) and to 20 μL CL substrate solution. These 20 μL enzyme solutions were prepared with 2 μL 1 μg/mL HRP, 5 μL 5 μM SA, 5 μL 5 μM Cu^{2+}, 5 μL 10 μM PPi, 5 μL 10 μM dNTP and certain volume of PBS. C) Effect of SA concentration on CL intensity of HRP-luminol-H_2O_2 system. D) Structural diagram of the CL detection of PPi or its related substances through PPi-EAR strategy. Error bars were estimated from three parallel experiments (n = 3).

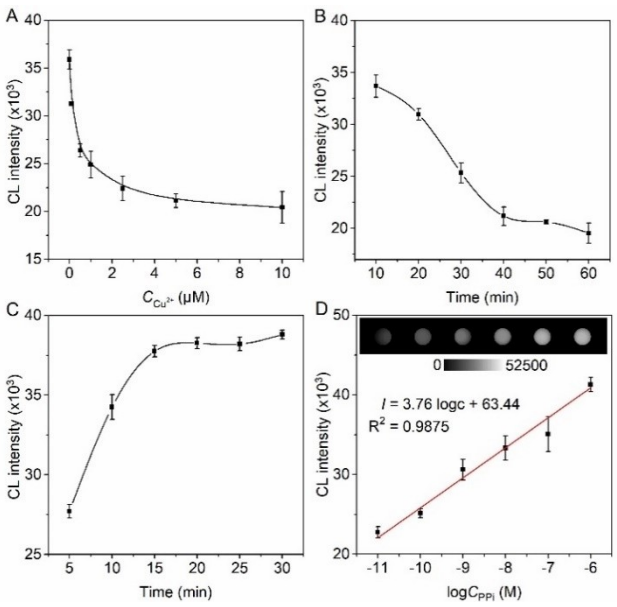

Figure 2. Effect of A) the concentration of Cu^{2+}, B) the inhibition time of HRP by Cu^{+}, and C) the reaction time of PPi with Cu^{2+} on CL intensity of the PPi-EAR strategy. D) CL intensity as the function of logarithm of PPi concentration. The PPi-EAR was constructed based on 20 μL enzyme solutions prepared with 2 μL 1 μg/mL HRP, 5 μL Cu^{2+}, 5 μL SA, 5 μL 10 μM PPi and certain volume of PBS. Error bars were estimated from three parallel experiments (n = 3).

reduction of SA to Cu^{+} via the formation of $CuPPi_2$, resulting in the retention of the strong CL signal (Figure 1B, column e). As dNTPs don't have electrons in the pyrophosphate radical, they cannot coordinate and protect Cu^{2+} from the reduction of SA,[16] thus no retention of the CL intensity is observed in the presence of dNTPs (Figure 1B, column f). The above results confirmed the feasibility of PPi-mediated HRP activity regulation. Obviously, this PPi-mediated enzyme activity regulation (PPi-EAR) could be used to construct CL detection methods for PPi or its related substances (Figure 1D). Here, PPi or its related substances induced the HRP activity regulation directly or indirectly to up-regulate the retention of active HRP, which subsequently generated CL signal for quantitative analysis.

To gain the best performance of PPi-EAR strategy, the concentration of Cu^{2+}, the inhibition time of HRP by Cu^{+}, and the coordination time of PPi with Cu^{2+} were optimized. The amount of Cu^{2+} was a vital parameter to determine the sensitivity of PPi-EAR. This was because the low amount of Cu^{2+} was unable to produce enough Cu^{+} to transform all active HRP to inactive HRP, leading to a high background, however, the excessive high amount of Cu^{2+} would produce supersaturated Cu^{+} for HRP inactivation, losing the regulation function of PPi on HRP activity. As shown in Figure 2A, the CL intensity was decreased by increasing the concentration of Cu^{2+}, it reached the minimum value at 5 μM Cu^{2+} and tended to be constant when Cu^{2+} concentration was higher than 5 μM, indicating the saturation concentration of Cu^{2+} to inhibit HRP activity in this work was 5 μM. In addition, to ensure the efficient inactivation of HRP by Cu^{+}, the inhibition time of HRP in the mixture of Cu^{2+} and SA was examined. The CL intensity decreased with the increase of incubation time, and reached the minimum value at about 40 min (Figure 2B). Therefore, 40 min was optimized as the inhibition time of HRP. Besides, PPi regulated the transformation of active HRP to inactive HRP based on the formation of $CuPPi_2$, thus the reaction time between PPi and Cu^{2+} was studied to ensure their complete reaction. Figure 2C showed the maximum CL intensity could be reached in 15 min, hence 15 min was selected for the coordination between PPi and Cu^{2+}.

The detection performance of PPi-EAR was evaluated firstly by examining its CL response to PPi. Under optimal conditions, PPi at different concentrations was successively mixed with Cu^{2+} and the mixture of HRP and SA, then the reaction mixtures were mixed with luminol and H_2O_2 to produce CL signal for quantitative analysis. As expected, the CL intensity increased with increasing the concentration

PPi, and the plot of CL signal versus the logarithm of PPi concentration from 10^{-11} to 10^{-6} M showed good linearity (Figure 2D). This result afforded the possibility to detect PPi related substances by the PPi-EAR strategy. For example, because PPi can be produced through the dNTP transformation in DNA polymerization, the PPi-EAR strategy can be applied with any DNA polymerization systems, such as RCA and PCR, without special design of base sequences.

Since RCA process was accompanied with the generation of PPi, the PPi-EAR could be extended to detect RCA-related molecules. As a proof of concept, the CL response to the primer

DNA (S3) of RCA was evaluated. Because PPi was produced through the dNTP transformation, the reaction time of RCA that determined the length of product DNA chain decided the amount of PPi as well as the final CL signal. As shown in Figure 3A, the CL intensity increased with increasing the RCA reaction time, while the background also increased within the increasing time, thus based on the signal-to-noise ratio, 1 h was selected as the optimum RCA time for rapid and sensitive detection. As expected, after the RCA product was successively mixed with Cu^{2+}, the mixture of HRP and SA, and the CL substrate, the CL intensity increased with the increasing primer concentration. The CL intensity exhibited a linear response toward the logarithmic primer concentration from 1 pM to 100 nM (Figure 3B), confirming the feasibility of PPi-EAR for the detection of RCA-related molecules.

By combining the PPi-EAR with a proximity binding-induced RCA (PB-RCA), a target-induced enzyme activity regulation was constructed for CL imaging detection of SARS-CoV-2 NP. Here, the double recognition of SARS-CoV-2 NP by a pair of antibody-DNA probes triggered the PB-RCA process. Afterwards, PPi produced in the PB-RCA implemented the enzyme activity regulation to retain HRP activity for CL signal generation (Figure 4A). Because the T-EAR based CLIA needed only solution addition but not washing and separation operations, it could realize high throughput screening detection of samples with SARS-CoV-2 NP on a 96-well plate. The CL intensity increased with the increasing concentration of SARS-CoV-2 NP. Besides, the generation time of CL signal to the plateau value was decreased with the increase of target concentration (Figure 4B). This phenomenon should be attributed to the low concentration of active HRP in the detection system (Figure S1). This phenomenon showed the detectable concentration of SARS-CoV-2 NP could be reduced lower by prolonging the CL signal collection time. The plot of CL signal versus the logarithm of SARS-CoV-2 NP concentration showed good linearity from 1 pg/mL to 100 ng/mL (13 fM to 1.3 nM) (Figure 4C). Compared with assays reported previously for SARS-CoV-2 protein detection, the method proposed in this work not only achieved high specificity and sensitivity, but also could be performed by a simple wash-free operation with small volume of samples (Table S2). In addition, the selectivity of the CLIA for SARS-CoV-2 NP was tested by comparing CL signals of samples containing different proteins, such as aminoterminal pro-brain natriuretic peptides (BNP), IgG, proprotein convertase subtilisin/kexin type 9 (PCSK-9), carcinoembryonic antigen (CEA), BSA and SARS-CoV-2 NP (Figure 4D). As expected, only the sample containing SARS-CoV-2 NP showed obvious CL output, demonstrating the proposed CLIA with T-EAR had good detection specificity for SARS-CoV-2 NP.

The accuracy of CLIA of SARS-CoV-2 NP was evaluated by the recovery tests conducted both in 10% fetal bovine serum (Table S3) and lung cancer patients' serum (Table S4). The detection results of SARS-CoV-2 NP with different concentrations showed the recovery rate ranged from 80.2 to 92.8%, indicating the acceptable reliability of the CLIA.

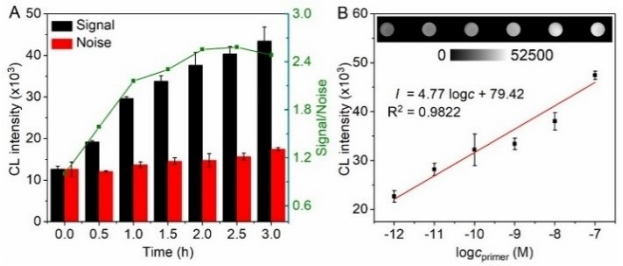

Figure 3. A) Effect of RCA reaction time on both CL intensity and signal-to-noise of PPi-EAR. B) CL intensity as the function of logarithm of primer concentration. Error bars were estimated from three parallel experiments (n = 3).

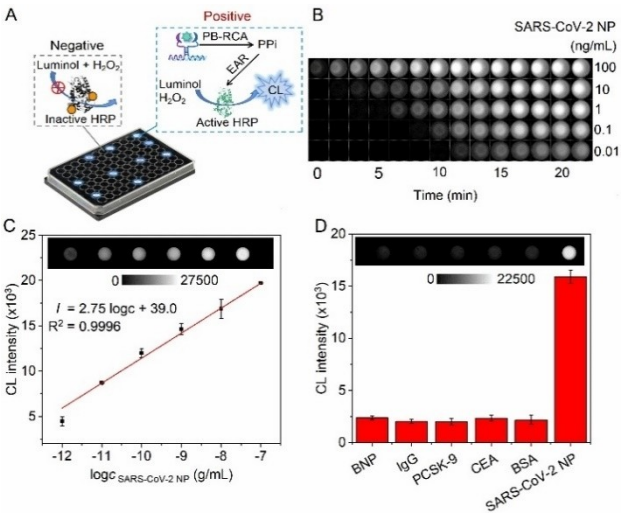

Figure 4. A) Schematic diagram of CLIA screening detection of samples with SARS-CoV-2 NP on a 96-well plate. B) CL imaging of SARS-CoV-2 NP at different concentrations. C) CL intensity as the function of logarithm of SARS-CoV-2 NP concentration. D) Specificity evaluation of CLIA to 1 ng/mL BNP, IgG, PCSK-9, CEA, BSA and SARS-CoV-2 NP. Error bars were estimated from 3 parallel experiments (n = 3).

Conclusion

In summary, a simple and sensitive CL imaging assay of SARS-CoV-2 NP was proposed based on a target-induced enzyme activity regulation strategy. The CLIA of SARS-CoV-2 NP was carried out in a test tube with four solution addition steps to go through a reaction process of target-induced proximity hybridization and primer release, primer-initiated RCA, RCA-assisted PPi production, PPi-mediated HRP activity regulation, and CL signal generation by active HRP. The CLIA could detect SARS-CoV-2 NP in a wide range from 1 pg/mL to 100 ng/mL (13 fM to 1.3 nM) with only 0.75 μL of sample. Additionally, the CLIA was able to screening detection of SARS-CoV-2 NP in multiple samples on the conventional 96-well plate. The proposed CLIA could detect SARS-CoV-2 NP with good sensitivity, simple operation, high throughput and acceptable accuracy, showing potential applicability in screening diagnosis of SARS-CoV-2 infections.

Experimental Section

Materials and reagents: HRP, $Cu(NO_3)_2$, sodium pyrophosphate, SA, tris(2-carboxyethyl) phosphine hydrochloride (TCEP) and 3-maleimidobenzoic N-hydroxysuccinimide ester (MBS) were purchased from Sigma-Aldrich Co. (Shanghai, China). Recombinant SARS-CoV-2 NP (Catalog No. FAP-IE012), murine monoclonal SARS-CoV-2 antibodies 2G1 (Ab1) and 2G2 (Ab2), BNP, and PCSK-9 were purchased from FANTIBODY (Chongqing, China). Splint R ligase, phi 29 DNA polymerase, dNTP, and their corresponding buffers were purchased from New England BioLabs (Beverly, MA, USA). Fetal bovine serum (FBS), BCA protein kit, silver stain kit, and TMB kit were bought from KeyGEN BioTECH Corp, Ltd. (Jiangsu, China). Hydrogen peroxide (30%), bovine serum albumin (BSA), and all DNA oligonucleotides (Table S1) were obtained from Sangon Biotechnology Co., Ltd. (Shanghai, China). The serum of lung cancer patient was provided by Nanjing Drum Tower Hospital (Jiangsu, China). Luminol solution was supplied by Antu Biological Co., Ltd. (China).

Preparation of circular DNA strand (S5): 1.6 μL padlock DNA (100 μM) and 2.4 μL primer DNA (100 μM) were added into 16 μL PBS (10 mM pH 7.2). The mixture was annealed at 95 °C for 5 min, and then slowly cooled to room temperature over 2 h. 2 μL splint R Ligase (25 U/μL) and 3 μL ligation buffer (containing 500 mM Tris-HCl, 100 mM $MgCl_2$, 10 mM ATP and 100 mM DTT) were added in the above mixture for padlock ligation by incubating 5 h at 25 °C with gentle vibration. After three times of ultrafiltration with 10 kDa tube at 12000 rmp, the product was mixed with 3 μL Exo III (100 U/μL) and 6 μL exonucleolytic buffer (CutSmart). Subsequently, the above solution was adjusted to a volume of 60 μL with 10 mM PBS (pH 7.2), and incubated at 37 °C for 5 h to produce circular DNA strand (S5). This reaction was terminated at 65 °C for 20 min, and the obtained S5 was stored at 4 °C before use.

Preparation of antibody-DNA probes: Antibody-DNA affinity probes were synthesized according to previous studies with slight modification.[14c] Briefly, 1 mg/mL Ab1 (or Ab2) was incubated with a 40-fold excess of MBS in 10 mM pH 7.2 PBS for 2 h at room temperature. Ab1-MBS (or Ab2-MBS) was obtained after removing extra MBS by ultrafiltration (30 kDa Millipore, 12000 rpm). Meanwhile, a 150-fold molar excess of TCEP was used to reduce thiolated DNA strands (S1 and S2, 10 μM) in PBS (10 mM, pH 5.5) for 2 h at room temperature, and the excess TCEP was removed by ultrafiltration (10 kDa Millipore, 12000 rpm). Then, the reduced S1 and S2 were severally reacted with Ab1-MBS and Ab2-MBS for 2 h at room temperature. Followed with a purification by ultrafiltration (50 kDa Millipore, 12000 rpm), Ab1-S1 and Ab2-S2 probes were obtained and calibrated through a BCA protein assay kit. These affinity probes were stored at −20 °C before use.

CL response to primer DNA: 0.5 μL DNA strand (S3) at different concentrations was mixed with 4.5 μL RCA solution and incubated for 1 h at 37 °C to process RCA. Here, RCA solution was prepared by mixing dNTPs (10 mM for each of dATP, dGTP, dCTP, and dTTP), BSA (20 mM), phi 29 polymerase (10 U/μL), 10×phi 29 reaction buffer, S5, and PBS (10 mM pH 7.2) in the volume ratios of 4:2:1:2:2:7. Then, 5 μL Cu^{2+} (5 μM) was added to the above mixture and incubated at room temperature for 15 min. Afterward, 10 μL enzyme solution (containing 0.2 μg/mL HRP and 2.5 μM sodium ascorbate, pH 7.2) were added for 40-min incubation at 37 °C. Later, 20 μL CL substrate, which was prepared by mixing 10 mM H_2O_2 and luminol solution in equal volume, was added to collect the CL images (BioSpectrum 615 Imaging System, UVP, USA) with an exposure time of 1 min.

CLIA of SARS-CoV-2 NP: 0.75 μL SARS-CoV-2 NP with different concentrations in PBS (10 mM, pH 7.2) or in 10% fetal bovine serum and lung cancer patients' serum was added into 4.25 μL assay solution and incubated for 1 h at 37 °C to process proximity binding-induced RCA. Here, the assay solution was prepared by mixing Ab1-S1 (10 ng/mL), Ab2-S2 (10 ng/mL), S3/S4 dsDNA (100 nM), dNTPs (10 mM for each of dATP, dGTP, dCTP, and dTTP), BSA (20 mM), phi 29 polymerase (10 U/μL), 10×phi 29 reaction buffer, and S5 in the volume ratios of 2:2:2:4:2:1:2:2. Then, same as CL response to DNA, 5 μL Cu^{2+} (5 μM), 10 μL enzyme solution and 20 μL CL substrate were added successively with 12-min incubation to produce CL image signal for SARS-CoV-2 NP detection. Here, CL images were collected with an exposure time of 30 s.

Calculation of recovery rate: After the CL images were collected, the mean CL intensity of each samples was read out through VisionWork. The measured concentration of target protein can be calculated by inputting the obtained CL intensity into the calibration curve (Figure 4C). By dividing the amount of the added concentration value of standard sample by the measured concentration value, the recovery rate could be obtained.

Acknowledgements

This work was financially supported by the National Natural Science Foundation of China (21827812), Independent Research Foundation from State Key Laboratory of Analytical Chemistry for Life Science (5431ZZXM2006), and the Fundamental Research Funds for the Central Universities (14380209).

Conflict of Interest

The authors declare no conflict of interest.

Data Availability Statement

The data that support the findings of this study are available in the supplementary material of this article.

Keywords: chemiluminescent imaging immunoassay · enzyme activity regulation · proximity hybridization · rolling circle amplification · SARS-CoV-2

[1] a) D. T. Ovanesyan, T. Gilboa, R. Lazarovits, A. Rosenthal, X. Yu, J. Z. Li, G. M. Church, D. R. Walt, *Anal. Chem.* **2021**, *93*, 5365–5370; b) P. H. Herroelen, G. A. Martens, D. De Smet, K. Swaerts, A. S. Decavele, *Am. J. Clin. Pathol.* **2020**, *154*, 610–619.

[2] a) M. M. Hatmal, W. Alshaer, M. A. I. Al-Hatamleh, M. Hatmal, O. Smadi, M. O. Taha, A. J. Oweida, J. C. Boer, R. Mohamud, M. Plebanski, *Cells* **2020**, *9*, 2638–2675; b) C. Chaimayo, B. Kaewnaphan, N. Tanlieng, N. Athipanyasilp, R. Sirijatuphat, M. Chayakulkeeree, N. Angkasekwinai, R. Sutthent, N. Puangpunngam, T. Tharmviboonsri, O. Pongraweewan, S. Chuthapisith, Y. Sirivatanauksorn, W. Kantakamalakul, N. Horthongkham, *Virol. J.* **2020**, *17*, 177; c) A. L. Ferreira, L. F. de Lima, M. T. Torres, W. R. de Araujo, C. de la Fuente-Nunez, *ACS Nano* **2021**,*15*, 17453–17462; d) T. A. Yano, T. Kajisa, M. Ono, Y. Miyasaka, Y. Hasegawa, A. Saito, K. Otsuka, A. Sakane, T. Sasaki, K. Yasutomo, R. Hamajima, Y. Kanai, T. Kobayashi, Y. Matsuura, M. Itonaga, T. Yasui, *Sci. Rep.* **2022**, *12*, 1060–1068.

[3] a) B. D. Grant, C. E. Anderson, J. R. Williford, L. F. Alonzo, V. A. Glukhova, D. S. Boyle, B. H. Weigl, K. P. Nichols, *Anal. Chem.* **2020**, *92*, 11305–11309; b) J. H. Lee, M. Choi, Y. Jung, S. K. Lee, C. S. Lee, J. Kim, J. Kim, N. H. Kim, B. T. Kim, H. G. Kim, *Biosens. Bioelectron.* **2021**, *171*, 112715.

[4] a) M. Norman, T. Gilboa, A. F. Ogata, A. M. Maley, L. Cohen, E. L. Busch, R. Lazarovits, C. P. Mao, Y. F. Cai, J. Zhang, J. E. Feldman, B. M. Hauser, T. M. Caradonna, B. Chen, A. G. Schmidt, G. Alter, R. C. Charles, E. T. Ryan, D. R. Walt, *Nat. Biomed. Eng.* **2020**, *4*, 1180–1187; b) A. F. Ogata, A. M. Maley, C. Wu, T. Gilboa, M. Norman, R. Lazarovits, C. P. Mao, G. Newton, M. Chang, K. Nguyen, M. Kamkaew, Q. Zhu, T. E. Gibson, E. T. Ryan, R. C. Charles, W. A. Marasco, D. R. Walt, *Clin. Chem.* **2020**, *66*, 1562–1572.

[5] a) H. Q. Zhang, F. Li, B. Dever, C. Wang, X. F. Li, X. C. Le, *Angew. Chem. Int. Ed.* **2013**, *52*, 10698–10705; *Angew. Chem.* **2013**, *125*, 10894–10902; b) H. Zhang, F. Li, B. Dever, X. F. Li, X. C. Le, *Chem. Rev.* **2013**, *113*, 2812–2841.

[6] a) M. Gullberg, S. M. Gustafsdottir, E. Schallmeiner, J. Jarvius, M. Bjarnegard, C. Betsholtz, U. Landegren, S. Fredrikson, *Proc. Nat. Acad. Sci.* **2004**, *101*, 8420–8424; b) O. Soderberg, M. Gullberg, M. Jarvius, K. Ridderstrale, K. J. Leuchowius, J. Jarvius, K. Wester, P. Hydbring, F. Bahram, L. G. Larsson, U. Landegren, *Nat. Methods* **2006**, *3*, 995–1000; c) I. Weibrecht, E. Lundin, S. Kiflemariam, M. Mignardi, I. Grundberg, C. Larsson, B. Koos, M. Nilsson, O. Soderberg, *Nat. Protoc.* **2013**, *8*, 355–372; d) F. Li, H. Zhang, Z. Wang, X. Li, X. F. Li, X. C. Le, *J. Am. Chem. Soc.* **2013**, *135*, 2443–2446; e) B. Koos, G. Cane, K. Grannas, L. Lof, L. Arngarden, J. Heldin, C. M. Clausson, A. Klaesson, M. K. Hirvonen, F. M. de Oliveira, V. O. Talibov, N. T. Pham, M. Auer, U. H. Danielson, J. Haybaeck, M. Kamali-Moghaddam, O. Soderberg, *Nat. Commun.* **2015**, *6*, 7294–7304.

[7] a) M. Zou, D. Li, R. Yuan, Y. Xiang, *Biosens. Bioelectron.* **2017**, *92*, 624–629; b) A. Porchetta, R. Ippodrino, B. Marini, A. Caruso, F. Caccuri, F. Ricci, *J. Am. Chem. Soc.* **2018**, *140*, 947–953; c) N. Li, L. Liu, M. H. Xiang, J. W. Liu, R. Q. Yu, J. H. Jiang, *Chem. Commun.* **2019**, *55*, 4387–4390.

[8] a) S. Bi, H. Zhou, S. S. Zhang, *Biosens. Bioelectron.* **2009**, *24*, 2961–2966; b) A. Tiwari, S. J. Dhoble, *Talanta* **2018**, *180*, 1–11.

[9] a) C. Zong, J. Wu, M. M. Liu, L. L. Yang, L. Liu, F. Yan, H. X. Ju, *Anal. Chem.* **2014**, *86*, 5573–5578; b) M. M. Liu, J. Wu, K. L. Yang, C. Zong, J. P. Lei, H. X. Ju, *Talanta* **2016**, *154*, 455–460; c) L. L. Zhou, L. L. Zhang, L. Yang, W. Ni, Y. Li, Y. H. Wu, *Biosens. Bioelectron.* **2021**, *173*, 112824.

[10] a) Q. Xiao, J. Wu, P. Y. Dang, H. X. Ju, *Anal. Chim. Acta* **2018**, *1032*, 130–137; b) F. Li, L. Guo, Z. M. Li, J. B. He, H. Cui, *Anal. Chem.* **2020**, *92*, 6827–6831.

[11] R. Zhang, J. Wu, H. Ao, J. L. Fu, B. Qiao, Q. Wu, H. X. Ju, *Anal. Chem.* **2021**, *93*, 9933–9938.

[12] a) N. X. Li, J. Y. Chen, M. Luo, C. H. Chen, X. H. Ji, Z. K. He, *Biosens. Bioelectron.* **2017**, *87*, 325–331; b) J. Li, X. Zhao, L. J. Chen, H. L. Qian, W. L. Wang, C. Yang, X. P. Yan, *Anal. Chem.* **2019**, *91*, 13191–13197.

[13] a) Y. H. Zhong, X. Y. Wu, J. Li, Q. C. Lan, Q. L. Jing, L. F. Min, C. L. Ren, X. Y. Hu, A. Lambert, Q. Cheng, Z. J. Yang, *Anal. Chim. Acta* **2019**, *1049*, 213–218; b) C. Zong, F. Jiang, X. Y. Wang, P. Li, L. R. Xu, H. Yang, *Biosens. Bioelectron.* **2021**, *177*, 112998; c) L. Z. Zhao, Y. Z. Fu, S. W. Ren, J. T. Cao, Y. M. Liu, *Biosens. Bioelectron.* **2021**, *171*, 112729.

[14] a) J. J. Deng, Q. Jiang, Y. X. Wang, L. F. Yang, P. Yu, L. Q. Mao, *Anal. Chem.* **2013**, *85*, 9409–9415; b) C. X. Chen, D. Zhao, J. Sun, X. R. Yang, *ACS Appl. Mater. Interfaces* **2016**, *8*, 29529–29535; c) H. Ao, W. W. Chen, J. Wu, W. C. Xiao, H. X. Ju, *Commun. Biol.* **2022**, *5*, 308.

[15] a) Y. L. Xianyu, K. Zhu, W. W. Chen, X. F. Wang, H. M. Zhao, J. S. Sun, Z. Wang, X. Y. Jiang, *Anal. Chem.* **2013**, *85*, 7029–7032; b) D. M. Shi, Y. Sun, L. Lin, C. J. Shi, G. F. Wang, X. J. Zhang, *Analyst* **2016**, *141*, 5549–5554.

[16] E. Ittah, D. Shamir, I. Zilbermann, E. Maimon, G. Yardeni, A. I. Shames, D. Meyerstein, *Inorg. Chim. Acta* **2013**, *405*, 72–76.

Manuscript received: May 9, 2022
Accepted manuscript online: August 16, 2022
Version of record online: ■■, ■■■

RESEARCH ARTICLE

A chemiluminescent imaging assay (CLIA) is designed for sensitive and simple detection of SARS-CoV-2 nucleocapsid protein (NP) based on a target-induced enzyme activity regulation (T-EAR) strategy. The T-EAR uses a proximity binding-induced RCA process to produce PPi and a PPi-mediated enzyme activity regulation process to retain HRP activity for signal generation. This CLIA is wash-free and can detect SARS-CoV-2 NP down to 1 pg/mL (13 fM) with only 0.75 μL of sample.

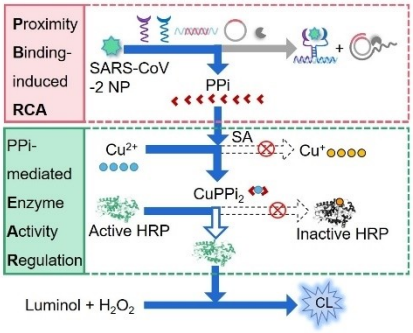

Y. Chen, H. Ao, W. Xiao, Prof. H. Ju, Prof. J. Wu**

1 – 7

Chemiluminescent Imaging Assay of SARS-CoV-2 Protein with Target-Induced Enzyme Activity Regulation